Biomass and Bioenergy xxx (xxxx) 107690

Contents lists available at ScienceDirect

Biomass and Bioenergy

journal homepage: www.elsevier.com/locate/biombioe

Sustainable cellulose/kraft lignin carbon xerogel applied to H_2O_2 electrogeneration using gas diffusion electrodes: Exploring the degradation of sulfamerazine in H_2O_2-based processes

Nicolas Perciani de Moraes [a, *], Julio César Lourenço [a], Robson da Silva Rocha [b], Liana Alvares Rodrigues [b, **], Marcos Roberto de Vasconcelos Lanza [a, ***]

[a] São Carlos Institute of Chemistry – University of São Paulo, Trabalhador São Carlense Avenue, 400 - Arnold Schimidt Park, São Carlos, São Paulo, Brazil
[b] Lorena School of Engineering - University of São Paulo, Campinho Municipal Road, Campinho, Lorena, São Paulo, Brazil

ARTICLE INFO

Keywords:
Kraft lignin
Cellulose
Carbon xerogel
Gas diffusion electrode
H_2O_2 electrogeneration
Photoelectro-fenton

ABSTRACT

This study investigated the application of cellulose/kraft lignin-derived carbon xerogels for hydrogen peroxide (H_2O_2) electrogeneration using gas diffusion electrodes, intending to develop cost-effective and environmentally sustainable H_2O_2-based processes for antibiotic degradation. Electrochemical characterization revealed that increasing the proportion of kraft lignin in the xerogels enhanced selectivity towards H_2O_2 electrogeneration, whereas calcination at elevated temperatures caused a positive shift in the onset potential of the oxygen reduction reactions (ORR), indicating a reduction in the energy requirements for H_2O_2 production. These enhancements are likely related to morphological and structural modifications induced by kraft lignin incorporation into the carbon xerogel, including changes in particle morphology, an increase in specific surface area, and the development of a microporous structure. Additionally, the synthesis process introduced oxygen and nitrogen-containing functional groups into the carbon xerogel, which are likely linked to the high selectivity obtained for H_2O_2 electrogeneration. When implemented in the fabrication of gas diffusion electrodes, the optimized carbon xerogel achieved a maximum H_2O_2 concentration of 700 mg L^{-1} within 1 h of electrolysis at a current density of 100 mA cm^{-2}. Among the techniques evaluated, the photoelectro-Fenton process demonstrated the highest efficiency for sulfamerazine removal, achieving complete degradation within 15 min and 75 % mineralization after 90 min.

1. Introduction

In recent years, the development of novel and efficient methodologies for the remediation of antibiotics in wastewater and natural water systems has gained critical importance. It is widely acknowledged that the widespread discharge of these compounds into aquatic environments can foster the appearance of antibiotic-resistant microorganisms, which poses a significant public health concern. This phenomenon not only exacerbates the prevalence and severity of infectious diseases but also increases the complexity and costs associated with medical treatments [1].

Building on insights from previous literature, the homogeneous photoelectro-Fenton process has emerged as a promising technique for the efficient degradation of various hazardous organic compounds, including antibiotics [2,3]. This method operates through the generation of hydroxyl active radicals via a cyclic reaction between hydrogen peroxide (H_2O_2) and ferrous iron ions (Fe^{2+}) under light irradiation, typically within the ultraviolet spectrum.

[2]. In this approach, hydrogen peroxide is produced in situ through the electrochemical reduction of O_2 at the cathode of the electrochemical system, thereby eliminating the costs and hazards associated with the handling, transportation, and storage of H_2O_2. Furthermore, the process optimizes the Fe^{2+}/Fe^{3+} redox cycle, reducing the required concentration of iron ions [4]. Exposure to light also initiates synergistic reactions that enhance hydroxyl radical production, including the direct photolysis of H_2O_2 and the photoreduction of Fe^{3+} ions, resulting in the subsequent release of additional hydroxyl radicals [5].

In this context, the photoelectro-Fenton process commonly employs gas diffusion electrodes (GDEs) for the effective electrochemical generation of H_2O_2 [6,7]. These electrodes typically consist of a permeable

* Corresponding author.
** Corresponding author.
*** Corresponding author.
E-mail addresses: nicolas.perciani@usp.br (N.P. de Moraes), liana.r@usp.br (L.A. Rodrigues), marcoslanza@usp.br (M.R. de Vasconcelos Lanza).

https://doi.org/10.1016/j.biombioe.2025.107690
Received 10 October 2024; Received in revised form 28 December 2024; Accepted 4 February 2025
0961-9534/

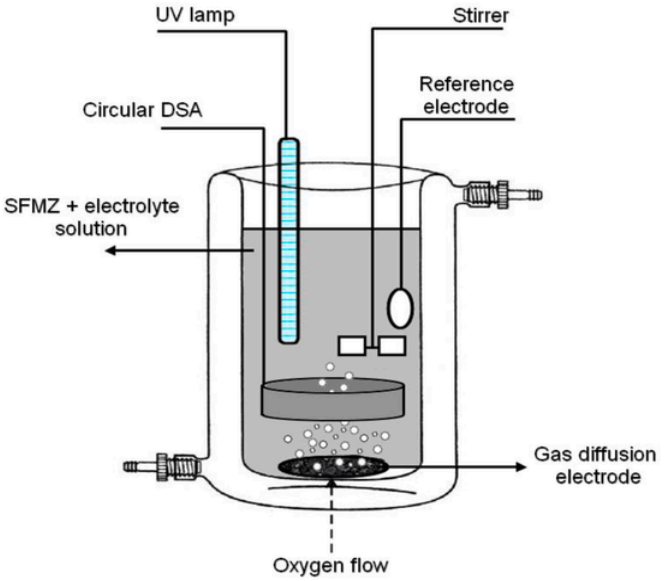

Fig. 1. – Schematics of the reactor employed.

catalyst layer interfaced with a liquid electrolyte, through which a gaseous stream of O_2 will be permeated [8–10]. Carbonaceous materials, including carbon nanotubes, graphene, graphene oxide, and carbon blacks, are extensively utilized in GDEs owing to their advantageous properties for the electrochemical reduction of O_2 to H_2O_2. These properties encompass a variety of surface functional groups, high thermal and chemical stability, a large specific surface area, and excellent electrical conductivity [8–14]. Nevertheless, the fabrication of these materials is often associated with high production costs, complex synthesis processes, and reliance on non-renewable carbon sources, such as petroleum industry by-products [12]. Consequently, the development of renewable carbonaceous materials to produce sustainable GDEs remains a relatively underexplored yet highly promising avenue of research. As an example, Wang et al. [15] developed cathodes based on pyrolyzed pitaya peels, achieving great H_2O_2 productivity (41.6 mg h^{-1} cm^{-2}) [15]. Similarly, Gao et al. [16] employed a peanut shell-derived biochar for H_2O_2 electrogeneration, with a stellar 87 % H_2O_2 electrosynthesis selectivity at neutral pH [16].

In this context, the primary natural precursors for sustainable carbon materials are biopolymers extracted from plant structures, most notably cellulose and lignin. Cellulose, recognized as the most abundant natural biopolymer, boasts an annual global production of approximately 1.5 trillion tons, positioning itself as a virtually inexhaustible source of raw material for the development of sustainable products [17,18]. Lignin, on the other hand, is an intricate three-dimensional polymer that mainly provides structural integrity to plant cell walls. This polymer is often obtained as a byproduct of various industrial processes, such as paper manufacturing and biofuel production, making its utilization as a sustainable resource a significant and ongoing challenge [19]. In this perspective, substantial attention has been directed toward the synthesis of cost-effective and sustainable carbon gels. These materials offer considerable versatility, with their structural properties readily tunable through variations in carbon precursors, synthesis parameters, drying techniques, and thermal treatment processes [20–23]. Despite the diverse applications of carbon gels derived across a range of fields, their potential for use in the fabrication of gas diffusion electrodes (GDEs) for H_2O_2 electrogeneration remains an underexplored area of research. Among the few examples available, Zhao et al. [24] developed a metal-organic-framework/carbon aerogel cathode for application in a solar photoelectro–Fenton process, exploring the degradation of Rhodamine B and dimethyl phthalate. The authors reported excellent degradation efficiency, however, the carbon aerogel employed was produced using resorcinol as a carbon precursor, diminishing the environmental appeal of the electrocatalyst [24].

Thus, the objective of this study is to investigate the development of novel gas diffusion electrodes (GDEs) derived from carbon xerogels synthesized using sustainable carbon sources, specifically Kraft lignin and cellulose. These electrodes are intended for application in the degradation of antibiotics, with a particular focus on the sulfamerazine molecule, through the homogeneous photoelectro-Fenton process.

2. Methodology

2.1. Synthesis of the carbonaceous materials and gas diffusion electrodes (GDEs)

Initially, pre-defined amounts of microcrystalline cellulose and dried kraft lignin were weighed, totaling 5 g of biomass. To evaluate the effect of the kraft lignin mass fraction on the final properties of the proposed composites, three materials were synthesized with compositions of 0 %, 25 %, and 50 % of kraft lignin. It is important to note that lignin mass fractions higher than 50 % led to the destabilization of the carbon gel during the gelation process and, therefore, could not be evaluated.

To create the carbon gel precursor, the weighed biomass was added to a solution (80 mL) containing 7 g of sodium hydroxide (97 % w/w) and 12 g of urea (99 % w/w). This mixture was cooled to −10 °C and stirred until complete dissolution of the biomass was achieved. The gelation of the precursor was carried out employing a coagulant solution (nitric acid, 2 mol L^{-1}), to which the precursor was added in a dropwise manner. The nitric acid acts as a non-solvent, permeating the precursor droplets and leading to the creation of cross-linked cellulose-lignin beads [25]. The resulting beads were separated from the nitric acid solution and dried for 24 h (60 °C). After drying, the beads were placed in sealed crucibles and calcined in a muffle furnace under an N_2 atmosphere. Multiple temperatures (300, 450, and 600 °C) were employed, and the calcination process was conducted for 30 min using a 10 °C min^{-1} heating ramp. The resulting carbon xerogels were then washed with deionized water until pH = 7 was achieved in the filtrate, dried, and sieved through a 325-mesh sieve. The materials will be identified as K-L/C *w*% (*y* ºC), where *w* represents the kraft lignin mass fraction and *y* represents the calcination temperature.

The production of the GDEs was carried out as follows: 2 g of the carbonaceous material was added to 25 mL of ethanol. After that, polytetrafuoroethylene (PTFE) was added to the mixture as a hydrophobic binder (1.42 g of a 60 % PTFE aqueous dispersion). The mixture was mechanically stirred for 30 min. The resulting slurry was evenly deposited onto the surface of a PX30-PW03 flat-weave carbon cloth (7 × 18 cm, geometric area of 126 cm^2). Another piece of carbon cloth with the same dimensions was then positioned on top of the deposited catalytic mass. This assembly was then subjected to a pressure of 2 tons and a temperature of 290 °C for 2 h, using a heat press. Finally, the obtained GDE was cut into a circular shape, with a 5 cm diameter and an area of 20 cm^2.

2.2. Characterization

Details about the characterization procedures can be found in the supplementary material.

2.3. Evaluation of H_2O_2 production and sulfamerazine degradation

The H_2O_2 production by the GDE developed was evaluated employing current densities of 25, 50, 75, and 100 mA cm^{-2} in a 250 mL electrochemical cell, using a 0.05 mol L^{-1} K_2SO_4 electrolyte at pH = 3 (ad-

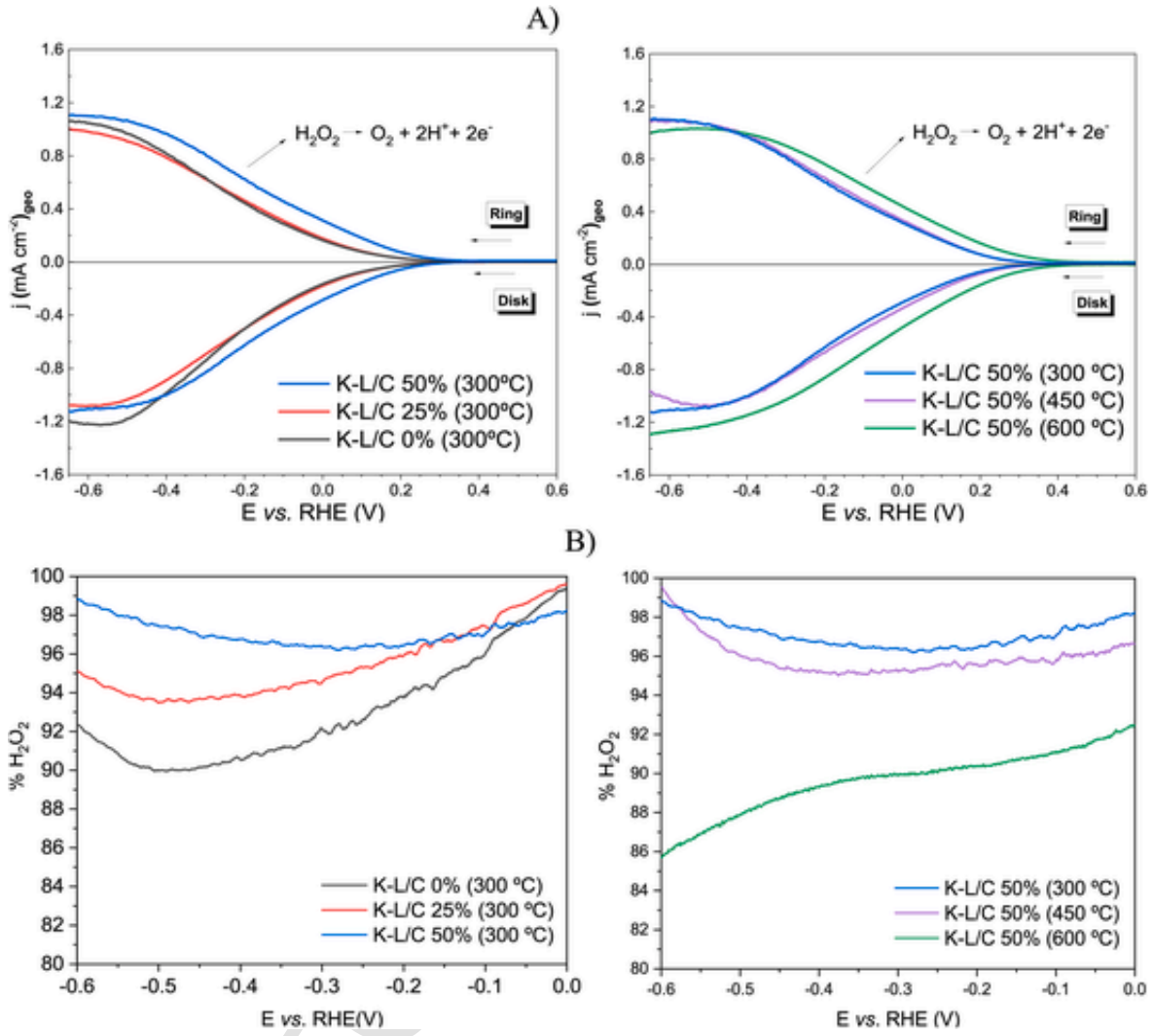

Fig. 2. A) Linear sweep voltammetry analysis (O_2-saturated 0.05 mol L^{-1} of K_2SO_4 electrolyte (pH = 3), 1600 rpm); B) % of H_2O_2 formation.

justed with H_2SO_4) under an O_2 flow of 0.05 L min^{-1}. During the process, 0.5 mL samples of the solution were added to 4 mL of acidic ammonium molybdate solution ($[(NH_4)_6Mo_7O_{24}.4H_2O]$ = 0.0024 mol L^{-1}, $[H_2SO_4]$ = 0.5 mol L^{-1}) to quantify the hydrogen peroxide electrogeneration over time. The resulting yellow-colored solution was analyzed at λ = 350 nm with a Shimadzu UV-1900 spectrophotometer.

The sulfamerazine (SFMZ) degradation tests were conducted using the same electrochemical cell and electrolyte employed in H_2O_2 electrogeneration experiments, using a 50 mg L^{-1} SFMZ initial concentration. A scheme of the system employed is shown in Fig. 1. For the kinetic analysis of the degradation reaction, chronopotentiometry was applied using a current density of 25 mA cm^{-2} for 90 min; the Fenton-based tests were conducted by adding 0.10 mmol of Fe^{2+} ($FeSO_4.7H_2O$) to the SFMZ solution. The radiation source for the UV-based tests consisted of an 11 W submergible UV-C lamp. The anodic oxidation of SFMZ was evaluated in the same manner described above; however, a nitrogen gas flow was used instead of oxygen. All the degradation tests were performed using the same gas diffusion electrode; after all the degradation tests were conducted, a new H_2O_2 electrogeneration experiment was performed in order to assess the stability of the GDE produced.

The SFMZ concentration during the tests was determined using an LC-20 AT Shimadzu HPLC with a C-18 column (Phenomenex Luna). The mobile phase consisted of 30 % deionized water and 70 % HPLC-grade acetonitrile (flow rate = 1 mL min^{-1}). Injection volume was maintained at 20 μL, with a retention time of 10 min. UV detection was carried out at λ = 270 nm. The determination of total organic carbon (TOC) content was achieved using a TOC-VCPN analyzer (Shimadzu).

3. Results and discussion

3.1. Characterization

Fig. 2 displays the results obtained by linear sweep voltammetry (O_2-saturated electrolyte), as well as the current efficiency for H_2O_2 production, which was determined using Equation (1) [26].

$$\%H_2O_2 = \frac{200 \bullet i_r}{i_d + \frac{i_r}{N}} \quad (1)$$

where i_r is the electrical current obtained on the ring of the RRDE, i_d is the electrical current obtained on the disk of the RRDE, and N is the electrode collection number (N = 0.37).

Concerning linear sweep voltammetry (LSV), it is crucial to identify the reactions that may occur at both the ring and disk components of the rotating electrode. Equations (2)–(6) depict the plausible reactions

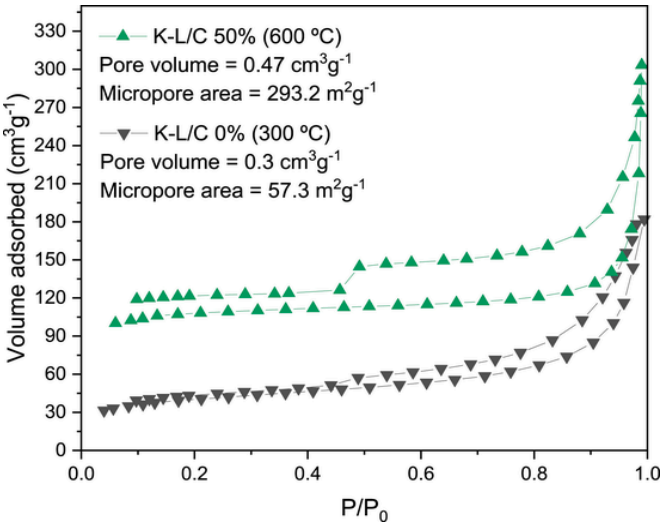

Fig. 3. Nitrogen adsorption-desorption isotherms for the K-L/C 0 % (300 °C) and K-L/C 50 % (600 °C).

Table 1
Specific surface areas (SSAs) obtained for the synthesized materials.

Material	SSA (m^2g^{-1})
K-L/C 0 % (300 °C)	140.6
K-L/C 25 % (300 °C)	197.7
K-L/C 50 % (300 °C)	269.3
K-L/C 50 % (450 °C)	290.1
K-L/C 50 % (600 °C)	363.2

that may take place throughout the LSV tests [27]. Consequently, it can be inferred that the sole reaction anticipated at the ring component of the electrode is the oxidation of the electrogenerated H_2O_2.

- *RRDE disk:*

$$O_2 + 4H^+ + 4e^- \rightarrow H_2O \quad (2)$$

$$O_2 + 2H^+ + 2e^- \rightarrow H_2O_2 \quad (3)$$

$$H_2O_2 + 2H^+ + 2e^- \rightarrow H_2O \quad (4)$$

$$2H^+ + 2e^- \rightarrow H_2 \quad (5)$$

- *RRDE ring:*

$$H_2O_2 \rightarrow O_2 + 2H^+ + 2e^- \quad (6)$$

Fig. 2 illustrates that the initial incorporation of kraft lignin did not yield significant advantages for the K-L/C 25 % material concerning H_2O_2 electrogeneration. This is evidenced by slightly reduced currents observed at both the ring and disk of the rotating ring-disk electrode (RRDE) during voltammetry, alongside a decrease in current efficiency. However, an increase in the kraft lignin mass fraction to 50 % (K-L/C 50 % (300 °C)) resulted in increased ring currents and higher current efficiency, indicating a greater electrogeneration of H_2O_2. It is also noticeable that the inclusion of the kraft lignin in this material led to a shift of approximately 0.05 V in the ORR onset toward more positive potentials, signifying a reduced energy demand for H_2O_2 production [6].

Regarding the calcination temperature, the use of a higher thermal treatment temperature (600 °C) resulted in an increased disk current. This behavior, however, led to a decrease in current efficiency for H_2O_2 generation. Nonetheless, a notable shift in the oxygen reduction reaction (ORR) onset potential was observed (approximately 0.07 V), indicating a lower energy requirement for the electrochemical generation of hydrogen peroxide. Consequently, the K-L/C 50 % (600 °C) material will be employed in the fabrication of the GDEs for the sulfamerazine degradation tests.

To enhance the comprehension of the results derived from the electrochemical tests, a comprehensive characterization of the developed materials was conducted. Fig. 3 displays the N_2 adsorption-desorption of the samples K-L/C 0 % (300 °C) and K-L/C 50 % (600 °C), whereas Table 1 presents the specific surface area (SSA) value for each material synthesized.

The isotherms corresponding to K-L/C 50 % (600 °C) and K-L/C 0 % (300 °C) are representative of a combination between types I-H4 and IV-H4, which are commonly observed for micro-mesoporous materials. The substantial adsorbed volume at low pressures reflects the presence of micropores, while the distinctive isotherm behavior at high pressures suggests the existence of a mesopore network [28]. The specific surface area is identified as a key parameter influencing the activity of carbonaceous materials in H_2O_2 electrogeneration, as an increased surface area provides more active sites for oxygen reduction reactions (ORR). Accordingly, the data in Table 1 aligns with the electrochemical evaluation results shown in Fig. 2.

The incorporation of kraft lignin and higher calcination temperatures was found to enhance the surface area of the materials, resulting in superior ORR activity for H_2O_2 electrogeneration, as evidenced by K-L/C 50 % (600 °C). Notably, the inclusion of kraft lignin in the K-L/C 50 % (600 °C) correlated with a significant 400 % increase in the micropore area of the composite. Lin et al. [29] reported that the inclusion of lignin in lignin-cellulose carbon aerogels resulted in the formation of micropores due to the thermal degradation of the lignin content during the calcination stage, which aligns perfectly with the results obtained in this work [29]. Furthermore, according to related literature, the presence of micropores can diminish the residence time of electrogenerated H_2O_2 on the surface of electrochemical catalysts, thereby preventing its further reduction to water and enhancing overall efficiency [8–10]. Thus, the observed modification is likely related to the enhanced efficiency exhibited by the K-L/C 50 % (600 °C) for H_2O_2 electrogeneration.

Fig. 4 shows the scanning electron micrographs (SEM) obtained for the prepared materials.

The micrographs reveal significant structural changes induced by the incorporation of kraft lignin into the prepared composites. As shown in Fig. 4A, the K-L/C 0 % (300 °C) material consists of thin, fiber-like particles, whereas the K-L/C 50 % (300 °C) exhibits particles arranged in a three-dimensional structure. According to related literature, the initial stages of lignin pyrolysis result in the formation of hard-shelled char with smooth particles; as the temperature increases (300-400 °C), a porous structure emerges in lignin-based materials due to the release of various gases (such as CO_2, CO, and H_2O) [30,31]. Therefore, the observed morphological transformation in K-L/C 50 % can be attributed to the inherent properties of lignin during the proposed thermal treatment. Taking into consideration the mechanism involved in oxygen reduction reactions, the development of such a porous structure is highly advantageous for the mass transport processes required for H_2O_2 electrogeneration, including the diffusion of O_2 molecules to the surface of the catalytic material [8–10,31,32[33]]. Furthermore, calcination at 600 °C seemingly resulted in the formation of larger macropores on the surface of the K-L/C 50 % (600 °C), further enhancing oxygen diffusion throughout the structure of the electrocatalyst.

Fig. 5 shows the infrared spectra collected for the materials developed, along with the XPS spectra and contact angle analysis for the K-L/C 0 % (300 °C), K-L/C 50 % (300 °C) and K-L/C 50 % (600 °C) samples.

Fig. 5A highlights a notable alteration in the chemical structure of the materials, as evidenced by the band positioned around 930 cm^{-1},

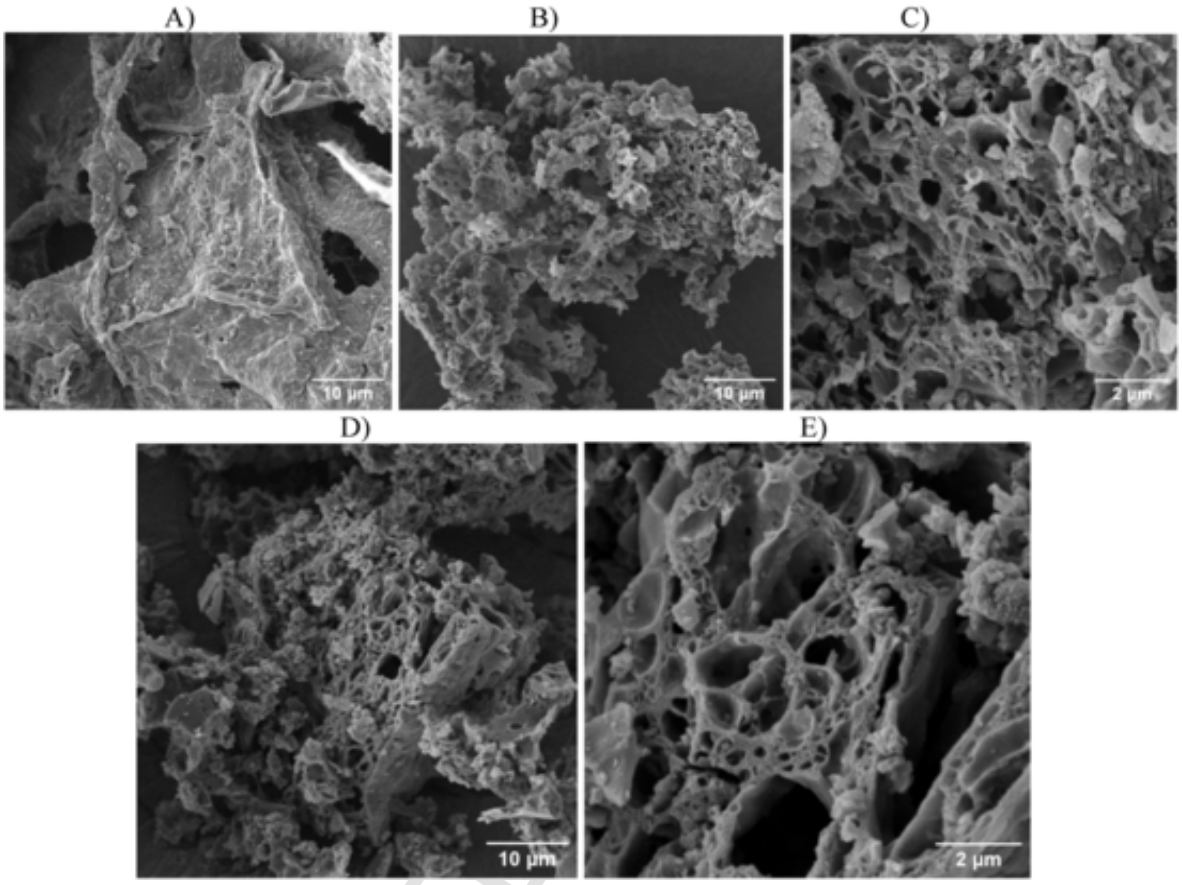

Fig. 4. – SEM for: A) K-L/C 0 % (300 °C) (5000x); B) K-L/C 50 % (300 °C) (5000x); C) K-L/C 50 % (300 °C) (20000x); D) K-L/C 50 % (600 °C) (5000x); E) K-L/C 50 % (600 °C) (20000x).

associated with the 1,4 β-glycosidic bonds of cellulose. The intensity of this band correlates with the amount of amorphous cellulose present, as the deformation of C-C-H, C-O-C, and C-C-O bonds contribute to the manifestation of this vibrational mode [34]. The addition of kraft lignin resulted in a significant reduction in the intensity of the 1,4 β-glycosidic band and an augmentation in the C-O band associated with C-O-C bonds (1040 cm^{-1}). These changes suggest a structural rearrangement within the cellulose component of the composite [34].

The bands observed at 1240, 1390, and 1480 cm^{-1} can be associated with the existence of amine superficial functional groups (C-N), while the band at approximately 1590 cm^{-1} can be attributed to both C=N bonds and C=C bonds within the lignin structure [35]. The formation of such nitrogen-based groups is likely a result of the substantial quantity of urea used in the synthesis of the carbon materials. Lastly, the band at 1145 cm^{-1} can be related to the existence of superficial oxygenated groups (C-O) on the surface of the prepared materials, which in turn can be attributed to both the inherent structure of the chosen biomasses and the influence of nitric acid, employed as an activator during the synthesis and thermal treatment processes [36]. Given that the gelation process relies on the permeation of nitric acid through the cellulose/kraft lignin droplets as an anti-solvent, it is expected that the gels obtained retain traces of this acid throughout the thermal treatment process. The use of nitric acid as an activator during the thermal treatment of carbonaceous matrices has been reported to contribute to the formation of various oxygenated functional groups, including carboxylic, lactonic, and phenolic groups [37].

As for the contact angle results (Fig. 5B), it can be noted that the inclusion of lignin into the composite led to a significant increase in the hydrophobicity of the composite, as a higher contact angle was obtained for both the K-L/C 50 % samples in comparison to the K-L/C 0 % (300 °C), which was considerably hydrophilic. This result can be attributed to the chemical modification of the composite's surface functional groups induced by the addition of lignin, as well as the morphological texturization achieved, as illustrated in Fig. 4. Enhancing the surface roughness of hydrophilic materials has been shown to improve their hydrophobic properties, leading to higher apparent contact angles, as observed for the K-L/C 50 % materials [38]. Recent literature has reported that controlling the hydrophilic/hydrophobic nature of catalytic materials is crucial for managing the interfacial conditions between electrodes and electrolytes, as excessive hydrophilicity or hydrophobicity can be detrimental to the overall efficiency of H_2O_2 generation [39]. In this context, Cordeiro-Junior et al. [12] reported that elevated hydrophilicity or hydrophobicity was linked to inferior efficiencies for H_2O_2 electrogeneration, through the evaluation of multiple carbon-based catalysts [12]. Thus, it can be stated that the K-L/C 50 % samples possess more balanced wettability properties, which could be also related to their superior H_2O_2 electrogeneration performance (Fig. 2).

Regarding the XPS results, the carbon C1s spectrum for all samples was deconvoluted into three distinct peaks. The first peak, located at 284.6 eV, corresponds to C–C bonds within the carbonaceous materials, while the adjacent peak at 286.2 eV is attributed to C–O bonds, consistent with the findings from the infrared (IR) analysis [40]. The smaller peak at 289 eV was attributed to O-C=O bondings, probably derived from the structure of the biomasses employed. Similarly, the two peaks deconvoluted from the O 1s spectra are linked to the presence of C-O (532.6 eV) and C=O (531.2 eV) bondings within the structure of the material, which is likely indicative of oxygenated surface groups [41–43]. However, it can be noted that the oxygen content of the K-L/C

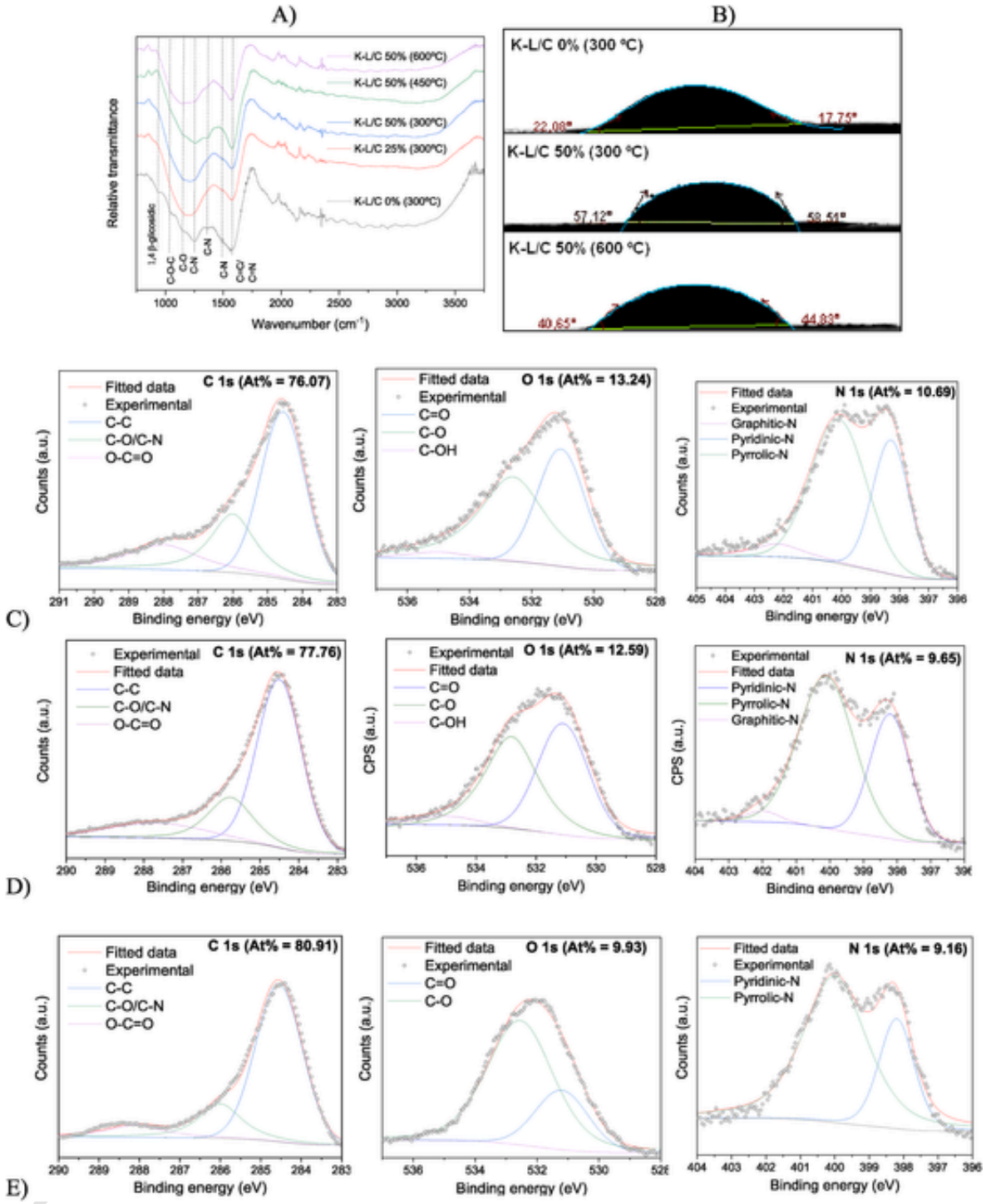

Fig. 5. A) Infrared spectra for the materials; B) Contact angle analysis for the materials; C) XPS spectra of the K-L/C 0 % (300 °C); D) XPS spectra of the K-L/C 50 % (300 °C); E) XPS spectra of the K-L/C 50 % (600 °C).

50 % (600 °C) sample is lower than the one observed for the material calcined at 300 °C, with a particular reduction of the C = O band, indicating that higher calcination temperatures led to the loss of some oxygenated functional groups. Finally, the nitrogen (N 1s) spectra for all samples exhibited two peaks of higher intensity. The first, located around 398.2 eV, is associated with superficial pyridinic nitrogen groups, while the second peak, at 400.2 eV, corresponds to pyrrolic nitrogen groups [31,32,44].

In the context of H_2O_2 electrogeneration, the interplay between oxygenated and nitrogen-based functional groups in enhancing efficiency is highly complex, being reportedly related to a myriad of factors, such as type of material, morphology, mass fraction of nitrogen (N) and oxygen (O), and the pH of the electrolysis process [30,31,45,46]. It is well-established that the presence of oxygenated functional groups can be linked to higher selectivity of H_2O_2 during electrolysis, whereas both the pyridinic and pyrrolic groups have been reported to influence positively the ORR onset and selectivity towards H_2O_2 during the oxygen re-

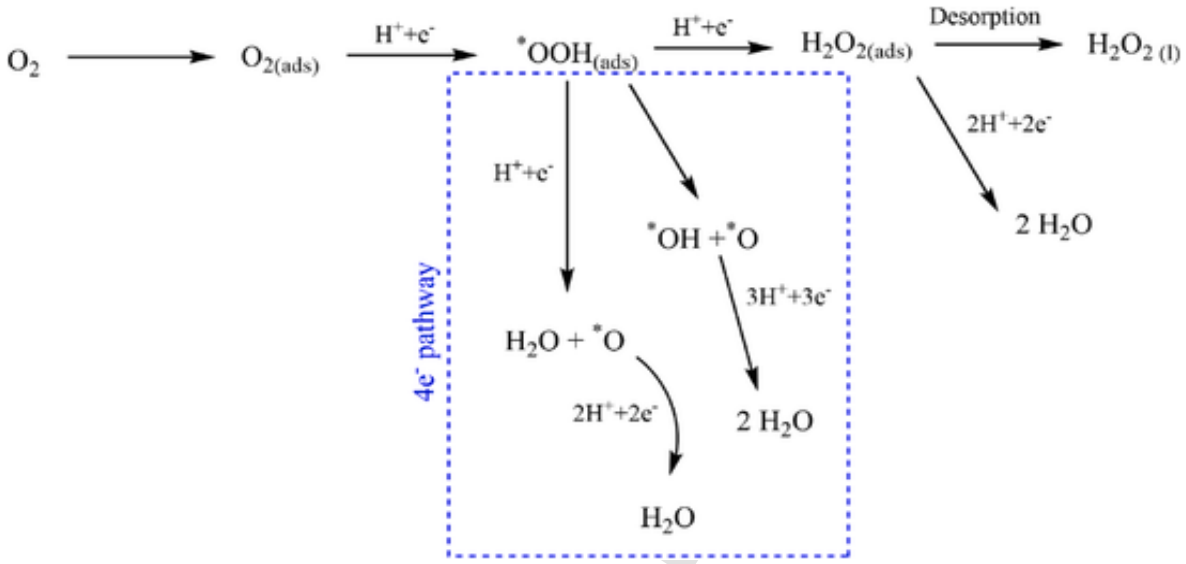

Fig. 6. Combined schematics of the $2e^-$ and $4e^-$ pathways for the electrochemical oxygen reduction reaction.

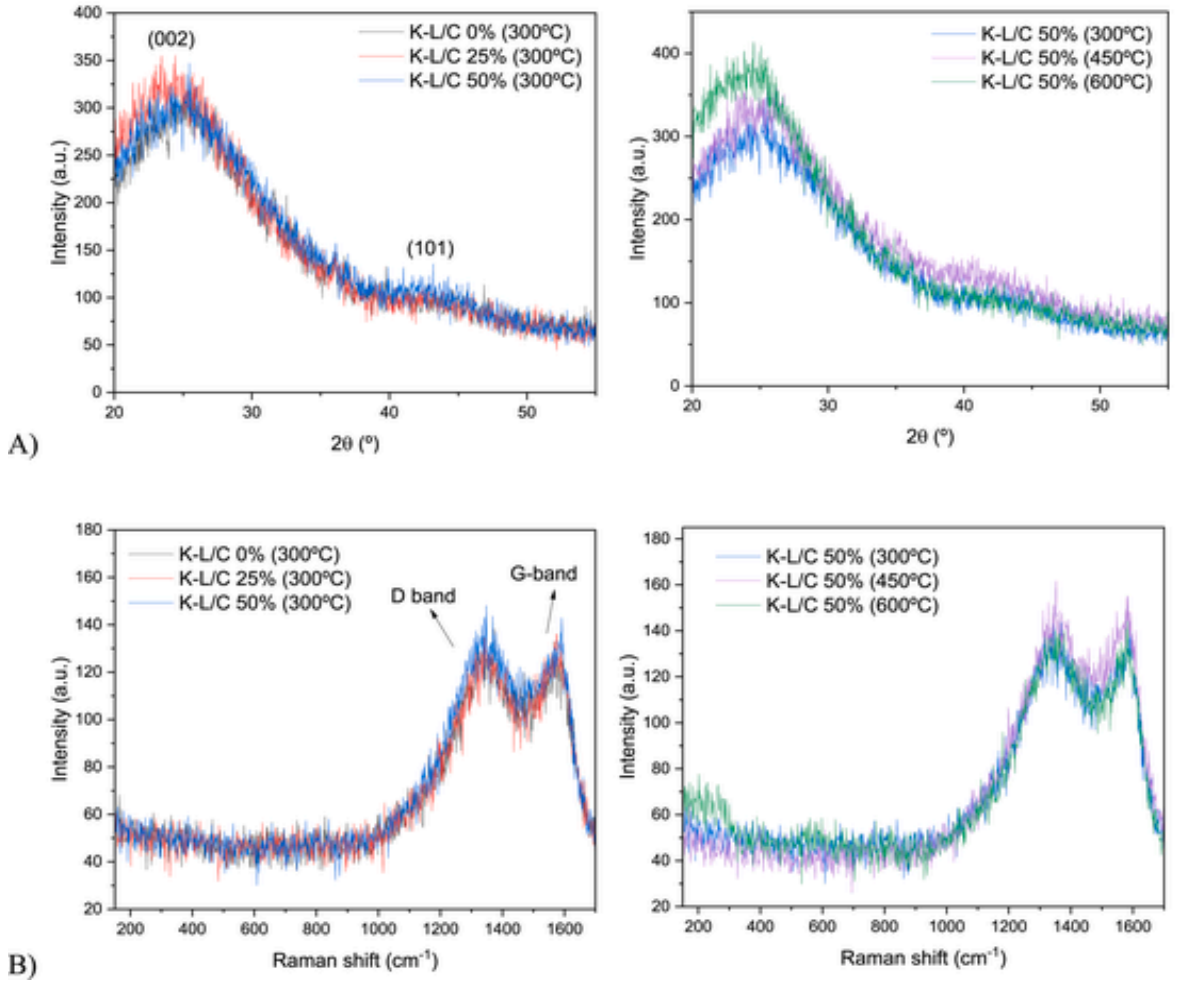

Fig. 7. A) X-ray diffractograms obtained for the synthesized samples; B) Raman spectra obtained for the synthesized samples.

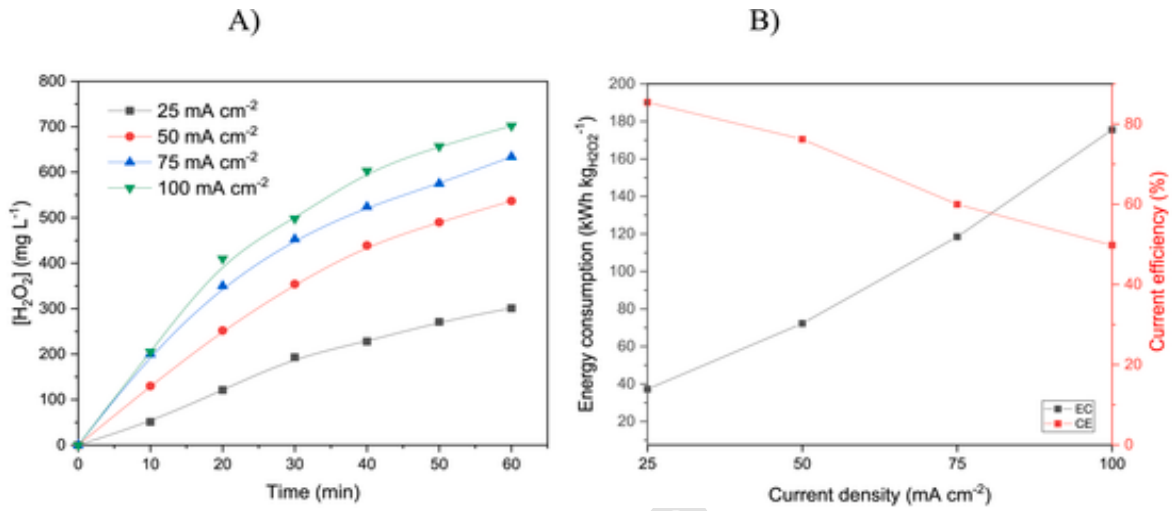

Fig. 8. A) H_2O_2 electrogeneration capacity for GDE produced using the K-L/C 50 % (600 °C) material (0.05M K_2SO_4, pH = 3, V = 0.25 L); B) Current efficiency and energy consumption achieved during the H_2O_2 electrogeneration tests employing different current densities.

duction reactions under specific conditions. This effect is attributed to the retention of the *OOH intermediate, hindering its further breakage into *O and *OH species in the 4e⁻ reduction pathway, as exemplified in the scheme provided in Fig. 6 [30,31,46–48]. However, Li et al. [30,31,46] also reported that an excessive nitrogen content can pose a negative influence on the selectivity for H_2O_2 electrogeneration, favoring the 4e⁻ ORR pathway [30,31,46]. Thus, the decrease of the oxygen content observed for the K-L/C 50 % (600 °C) sample may be related to both its improved ORR onset and lower selectivity for H_2O_2, as it may have changed the complex interplay involved in the 2e⁻ ORR pathway promoted by the functional groups available.

Fig. 7 shows the results of the X-ray diffraction and Raman spectrometry obtained for the synthesized materials.

In Fig. 7A, the prominent characteristic bands at $2\theta = 24.3°$ and 44° correspond to the (002) and (101) planes of hexagonal carbon, respectively [49]. The position and low intensity of these bands suggest that the synthesized samples are primarily amorphous with low levels of graphitization. This observation is consistent with the fact that nitrogen doping in carbon materials, as observed in the XPS analyses (Fig. 5C, D, and 5E), introduces defect sites and disrupts the carbon lattice structure, thereby hindering the formation of well-ordered graphitic domains [30,31,46].

The Raman spectra further confirm the amorphous nature of the synthesized materials, as only two peaks, located at 1340 cm^{-1} and 1560 cm^{-1}, can be observed. These peaks are related to the D band and G band of the carbonaceous structure, respectively. The D band is associated with vacancies and impurities leading to a loss in the hexagonal symmetry of the carbon structure, representing disordered sp^2-hybridized carbon, whereas the G band signifies the presence of a graphitic structure, corresponding to the $2E_{2g}$ vibrational mode of a two-dimensional C–C bond stretching in the network structure [50].

3.2. Degradation tests

Considering all the information gathered in Section 3.1, the K-L/C 50 % (600 °C) was chosen for the production and application of the GDE described in Section 2.1. Firstly, the H_2O_2 electrogeneration capacity using the GDE was evaluated, along with the current efficiency and energy consumption achieved. The results are presented in Fig. 8.

The assessment of H_2O_2 electrogeneration over time in correlation with the cell potential enables the calculation of the current efficiency (CE) and energy consumption (EC) parameters, employing Equations (7) and (8), respectively [51].

$$CE_{H2O2}\,(\%) = \frac{2FC_{H2O2}V}{it}\ x\ 100 \tag{7}$$

$$EC\ \left(kWh\ kg^{-1}_{H2O2}\right) = \frac{i\ E_{cell}t}{m\ 1000} \tag{8}$$

where i is the current applied (A) to the system, t is the duration of the H_2O_2 electrogeneration test, E_{cell} is the potential of the electrochemical cell during each experiment (V), m represents the mass of electrogenerated H_2O_2 (kg), C_{H2O2} represents the concentration of H_2O_2 (mol L^{-1}), F is equal to the Faraday constant (96.49 C mol^{-1}), and V is the volume of electrolyte used in each test (L).

The results demonstrate that the GDE fabricated using the K-L/C 50 % (600 °C) was able to generate up to 700 mg L^{-1} of hydrogen peroxide in the proposed reactor, after 1 h of electrolysis. A progressive increase in current density led to higher concentrations of electrogenerated hydrogen peroxide, as anticipated. Nevertheless, the increase in applied current density also resulted in a reduction in current efficiency. This phenomenon could be attributed to excessive energy supplied to the system, which may promote parallel secondary reactions alongside hydrogen peroxide generation, such as its reduction via the 2e⁻ pathway, leading to the formation of H_2O (Fig. 6) [7]. Among the current densities applied during the electrogeneration process, the condition of 25 mA cm^{-2} exhibited the highest current efficiency and the lowest energy consumption. Consequently, this condition was selected for subsequent sulfamerazine degradation experiments.

The results for the sulfamerazine degradation tests employing the K-L/C 50 % (600 °C) GDE are displayed in Fig. 9. Table S1 shows the result of the linear fitting of the data obtained to a pseudo-1st-order kinetic model.

Firstly, the UV-based degradation process obtained the smallest mineralization percentage (4 %) and apparent reaction rate ($k_{app\ (UV)}$ = 0.003 min^{-1}), indicating that the UV radiation alone is not sufficient to efficiently degrade the SFMZ molecule. Observing Fig. 9A, it is noticeable that the efficiency of SFMZ removal solely by the electrogenerated hydrogen peroxide closely resembles that of anodic oxidation, as both these processes achieved similar k_{app} values ($k_{app(AO)}$ = 0.027 min^{-1} and $k_{app(H2O2)}$ = 0.030 min^{-1}). This similarity suggests that, on its own, the electrogenerated H_2O_2 lacks a strong oxidation potential for the degradation of the sulfamerazine molecule, even if a slightly

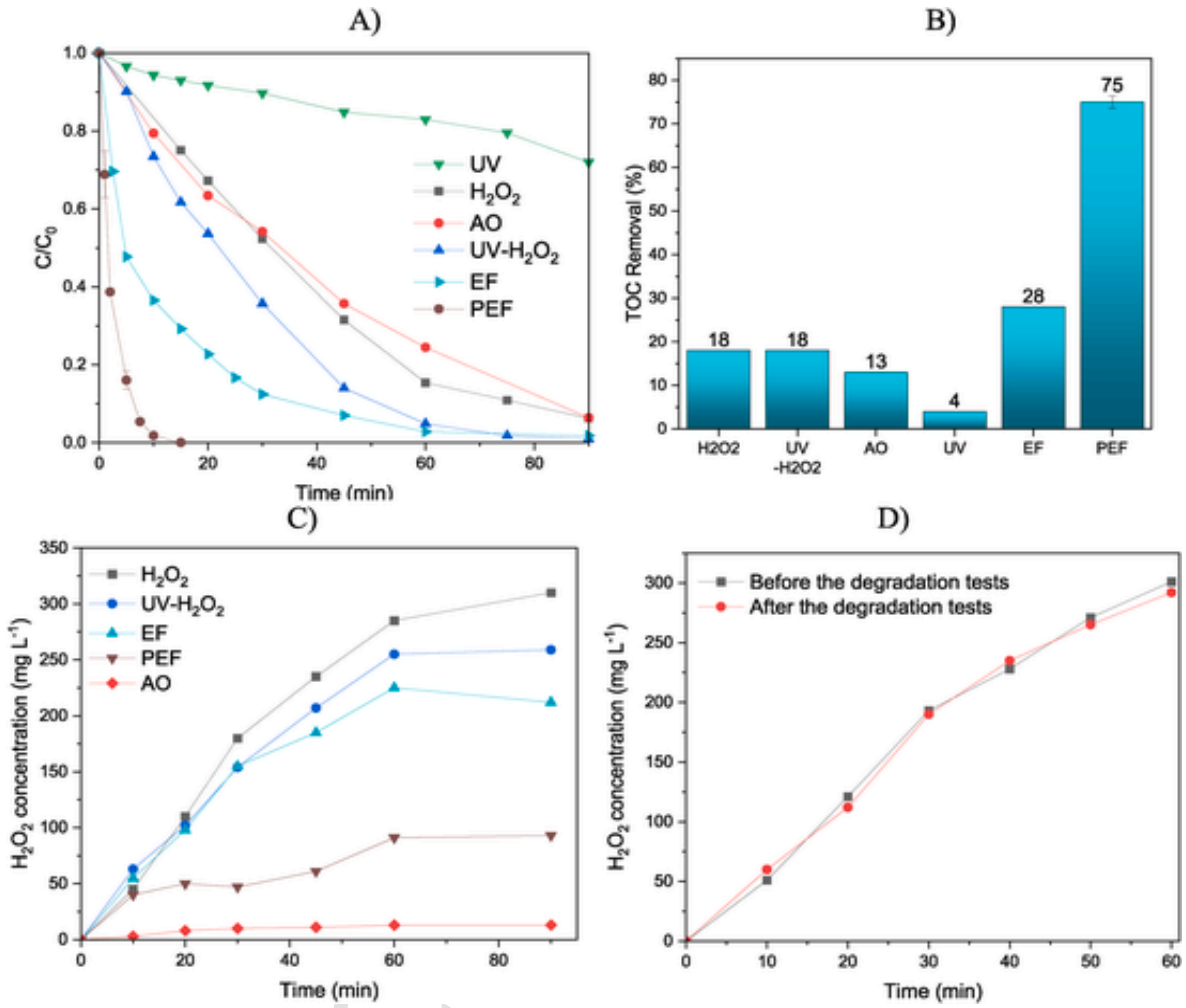

Fig. 9. A) Results for the sulfamerazine degradation tests (0.05M K_2SO_4, pH = 3, V = 0.25 L, C_{SFMZ} = 50 mg L^{-1}, Current density = 25 mA cm^{-2}, AO = Anodic oxidation, EF = electro-Fenton, PEF = photoelectro-Fenton); B) TOC results for the degradation tests after 90 min; C) H_2O_2 concentration during each degradation test; D) H_2O_2 electrogeneration before and after all the SFMZ degradation tests.

higher TOC removal was obtained in the H_2O_2 test. Further evidence of the lower efficiency of this test can be noticed in Fig. 9C, as the concentration of H_2O_2 during the SFMZ degradation test remains virtually the same as the one observed in the H_2O_2 electrogeneration test conducted previously, indicating that the hydrogen peroxide available was not converted into active hydroxyl radical.

Subsequently, the electro-Fenton and UV-H_2O_2 degradation processes were examined. In these tests, there was a notable improvement in the degradation of SFMZ, as depicted in Fig. 9A. In the case of the UV-H_2O_2 process, an improved apparent reaction rate ($k_{app(UV-H2O2)}$ = 0.050 min^{-1}) was obtained, which can be attributed to the effect of UVC light irradiaiton, which facilitates the generation of homogeneous hydroxyl radicals through the photolysis of H_2O_2. However, no enhancement was observed in the TOC removal, indicating that the sole inclusion of the UV radiation was not enough to efficiently remove the SFMZ and its degradation intermediates from the system. As for the electro-Fenton process, the introduction of ferrous iron into the system is known to catalyze the formation of hydroxyl radicals via Fenton-like reactions, further amplifying the efficiency of the degradation process [5]. Thus, a higher apparent reaction rate ($k_{app\ (EF)}$ = 0.06 min^{-1}) was achieved for the SFMZ degradation through the electro-Fenton process, accompanied by a higher mineralization percentage (28 %). Fig. 9C confirms the behavior described above for the UV-H_2O_2 and electro-Fenton tests, as the concentration of H_2O_2 during these degradation tests was clearly reduced, indicating the successful formation of hydroxyl radicals through the mechanisms proposed.

Finally, the photoelectro-Fenton process achieved the highest degradation efficiency and mineralization capacity among the tests performed, due to the synergistic effect of the UV light and Fenton-like reactions to produce hydroxyl radicals through the conversion of electrogenerated H_2O_2, as evidenced by the low concentration of hydrogen peroxide observed during the PEF test (Fig. 9C). In this case, the enhanced mineralization of PEF is attributed to the optimization of the Fenton reaction between H_2O_2 and Fe^{2+} by additional regeneration of Fe^{2+} ions through additional mechanisms induced by light irradiation. This can be achieved through the photoreduction of $Fe(OH)^{2+}$, which is the main iron-based species at pH between 2.8 and 3.5, and the photodecarboxylation of Fe(III)-carboxylate species [2]. Therefore, the highest k_{app} value ($k_{app\ (PEF)}$ = 0.420 min^{-1}) and TOC removal (75 %) were observed in this test, highlighting the favorable synergy between the individual processes composing the photoelectro-Fenton method for SFMZ degradation.

Regarding the stability of the fabricated GDE, Fig. 9D shows a comparison between H_2O_2 electrogeneration tests before and after all the degradation tests were performed. The results show that the GDE was able to maintain its H_2O_2 electrogeneration capacity after the SFMZ degradation tests, indicating good stability for application under multiple cycles.

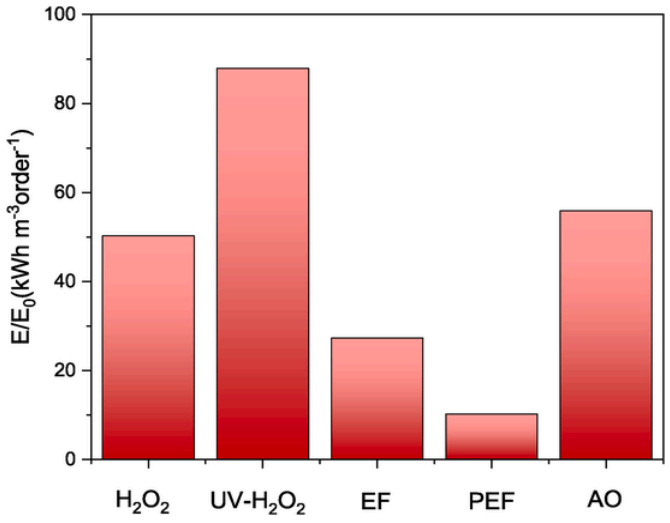

Fig. 10. Electrical energy consumed to reduce the concentration of SFMZ under different processes.

Equation (9) was used to assess and compare the treatment methods based on their electrical energy consumption per order of decrease in pollutant concentration (E/E_O). In this equation, E_{cell} represents the cell potential in volts (V), P_{lamp} is the power of the UVC lamp in watts (W), k_{app} is the pseudo-first-order rate constant (s^{-1}), and V is the volume in cubic meters (m^3) [52]. Fig. 10 shows the results obtained.

$$E/E_0 = 0.000639\frac{(E_{cell} + P_{lamp})}{Vk_{app}} \quad (9)$$

The superior performance of the PEF process is evident, with the lowest E/E_O value (10.2 kWh m^{-3} $order^{-1}$). In contrast, the individual and binary processes exhibited significantly higher energy consumption (the individual photolysis process, not shown in Fig. 10, achieved an E/E_O value of 937.2 kWh m^{-3} $order^{-1}$). This makes the PEF process the most advantageous among the methodologies studied, as the reduced energy required to achieve a one-order magnitude reduction in the SFMZ concentration highlights the environmentally friendly and cost-effective nature of this process.

4. Conclusion

Regarding the kraft lignin/cellulose carbon xerogel, it was concluded that both the kraft lignin mass fraction and calcination temperature exerted a significant influence on the electrochemical and structural properties of the composites. A higher kraft lignin content (50 %) combined with an elevated calcination temperature (600 °C) resulted in a material with advantageous properties for the H_2O_2 electrogeneration process, probably due to morphological modifications and a significant increase in the specific surface area. The application of the optimized material in the fabrication of gas diffusion electrodes was successful regarding the electrochemical generation of H_2O_2, achieving H_2O_2 concentrations of approximately 700 mg L^{-1} (100 mA cm^{-2}) after 1 h of electrogeneration. Finally, the application of the sustainable GDE in sulfamerazine degradation proved to be highly effective, in particular for the photoelectro-Fenton process. This method was able to harness the synergistic interaction between Fenton reactions and UV irradiation, achieving complete degradation of the SFMZ within 15 min and 75 % mineralization after 90 min.

Ethical approval

Not applicable.

Uncited References

[33].

CRediT authorship contribution statement

Nicolas Perciani de Moraes: Writing – review & editing, Writing – original draft, Visualization, Validation, Software, Methodology, Investigation, Formal analysis, Conceptualization. **Julio César Lourenço:** Writing – original draft, Visualization, Validation, Software, Methodology, Investigation, Formal analysis. **Robson da Silva Rocha:** Writing – original draft, Visualization, Validation, Software, Methodology, Investigation, Formal analysis. **Liana Alvares Rodrigues:** Writing – review & editing, Writing – original draft, Visualization, Validation, Supervision, Resources, Project administration, Methodology, Investigation, Funding acquisition, Formal analysis, Conceptualization. **Marcos Roberto de Vasconcelos Lanza:** Writing – review & editing, Writing – original draft, Visualization, Validation, Supervision, Resources, Project administration, Methodology, Investigation, Funding acquisition, Formal analysis, Conceptualization.

Funding

This study was financed, in part, by the São Paulo Research Foundation (FAPESP), Brasil (Process Number #2014/50945–4, #2017/10118–0, #2021/12053–8, #2022/12895–1 and #2022/04058–2) and by the National Council for Scientific and Technological Development – CNPq (Grants #465571/2014–0 and #303943/2021–1).

Data availability

Data will be made available on request.

Appendix A. Supplementary data

Supplementary data to this article can be found online at https://doi.org/10.1016/j.biombioe.2025.107690.

References

[1] Z. Wei, J. Liu, W. Shangguan, A review on photocatalysis in antibiotic wastewater: pollutant degradation and hydrogen production, Chin. J. Catal. 41 (2020) 1440–1450, https://doi.org/10.1016/S1872-2067(19)63448-0.
[2] E. Brillas, A review on the photoelectro-Fenton process as efficient electrochemical advanced oxidation for wastewater remediation. Treatment with UV light, sunlight, and coupling with conventional and other photo-assisted advanced technologies, Chemosphere (2020), https://doi.org/10.1016/j.chemosphere.2020.126198.
[3] A. Hosseini, H. karimi, J. Foroughi, M.M. Sabzehmeidani, M. Ghaedi, Heterogeneous photoelectro-Fenton using ZnO and TiO2 thin film as photocatalyst for photocatalytic degradation Malachite Green, Appl. Surf. Sci. Adv. 6 (2021), https://doi.org/10.1016/j.apsadv.2021.100126.
[4] S. Rahim Pouran, A.R. Abdul Aziz, W.M.A. Wan Daud, Review on the main advances in photo-Fenton oxidation system for recalcitrant wastewaters, J. Ind. Eng. Chem. 21 (2015) 53–69, https://doi.org/10.1016/j.jiec.2014.05.005.
[5] M. hui Zhang, H. Dong, L. Zhao, D. xi Wang, D. Meng, A review on Fenton process for organic wastewater treatment based on optimization perspective, Sci. Total Environ. 670 (2019) 110–121, https://doi.org/10.1016/j.scitotenv.2019.03.180.
[6] G.V. Fortunato, M.S. Kronka, A.J. dos Santos, M. Ledendecker, M.R.V. Lanza, Low Pd loadings onto Printex L6: synthesis, characterization and performance towards H2O2 generation for electrochemical water treatment technologies, Chemosphere 259 (2020) 127523, https://doi.org/10.1016/j.chemosphere.2020.127523.
[7] Ricardo Bertholo Valim, J.F. Carneiro, J.C. Lourenço, P. Hammer, M.C. dos Santos, L.A. Rodrigues, R. Bertazzoli, M.R. de Vasconcelos Lanza, R. da Silva Rocha, Synthesis of Nb2O5/C for H2O2 electrogeneration and its application for the

degradation of levofloxacin, J. Appl. Electrochem. (2023), https://doi.org/10.1007/s10800-023-01975-z.
[8] J. Wang, C. Li, M. Rauf, H. Luo, X. Sun, Y. Jiang, Gas diffusion electrodes for H2O2 production and their applications for electrochemical degradation of organic pollutants in water: a review, Sci. Total Environ. 759 (2021) 143459, https://doi.org/10.1016/j.scitotenv.2020.143459.
[9] N. Wang, S. Ma, P. Zuo, J. Duan, B. Hou, Recent progress of electrochemical production of hydrogen peroxide by two-electron oxygen reduction reaction, Adv. Sci. 8 (2021) 1–26, https://doi.org/10.1002/advs.202100076.
[10] Y. Wang, J. Chen, J. Gao, H. Meng, S. Chai, Y. Jian, L. Shi, Yanbin Wang, C. He, Selective electrochemical H2O2 generation on the graphene aerogel for efficient electro-Fenton degradation of ciprofloxacin, Sep. Purif. Technol. 272 (2021) 118884, https://doi.org/10.1016/j.seppur.2021.118884.
[11] Y. Bu, Y. Wang, G.F. Han, Y. Zhao, X. Ge, F. Li, Z. Zhang, Q. Zhong, J.B. Baek, Carbon-based electrocatalysts for efficient hydrogen peroxide production, Adv. Mater. 33 (2021) 1–19, https://doi.org/10.1002/adma.202103266.
[12] P.J.M. Cordeiro-Junior, M.S. Kronka, L.A. Goulart, N.C. Veríssimo, L.H. Mascaro, M.C. dos Santos, R. Bertazzoli, M.R. de V. Lanza, Catalysis of oxygen reduction reaction for H2O2 electrogeneration: the impact of different conductive carbon matrices and their physicochemical properties, J. Catal. 392 (2020) 56–68, https://doi.org/10.1016/j.jcat.2020.09.020.
[13] J. Lu, X. Liu, Q. Chen, J. Zhou, Coupling effect of nitrogen-doped carbon black and carbon nanotube in assembly gas diffusion electrode for H2O2 electro-generation and recalcitrant pollutant degradation, Sep. Purif. Technol. 265 (2021) 118493, https://doi.org/10.1016/j.seppur.2021.118493.
[14] R.S. Rocha, R.B. Valim, L.C. Trevelin, J.R. Steter, J.F. Carneiro, J.C. Forti, R. Bertazzoli, M.R.V. Lanza, Electrocatalysis of hydrogen peroxide generation using oxygen-fed gas diffusion electrodes made of carbon black modified with quinone compounds, Electrocatalysis 11 (2020) 338–346, https://doi.org/10.1007/s12678-020-00591-1.
[15] S. Wang, H. Liu, D. Ye, Q. Lan, X. Zhu, Y. Yang, R. Chen, Q. Liao, Oxygen self-doping formicary-like electrocatalyst with ultrahigh specific surface area derived from waste pitaya peels for high-yield H2O2 electrosynthesis and efficient electro-Fenton degradation, Sep. Purif. Technol. 289 (2022) 120687, https://doi.org/10.1016/j.seppur.2022.120687.
[16] M. Gao, Z.Y. Wang, Y.R. Yuan, W.W. Li, H.Q. Liu, T.Y. Huang, Ball-milled biochar for efficient neutral electrosynthesis of hydrogen peroxide, Chem. Eng. J. 434 (2022) 134788, https://doi.org/10.1016/j.cej.2022.134788.
[17] B. Baghaei, M. Skrifvars, All-cellulose composites: a review of recent studies on structure, properties and applications, Molecules 25 (2020), https://doi.org/10.3390/MOLECULES25122836.
[18] A. Sharma, M. Thakur, M. Bhattacharya, T. Mandal, S. Goswami, Commercial application of cellulose nano-composites – a review, Biotechnol. Reports 21 (2019) e00316, https://doi.org/10.1016/j.btre.2019.e00316.
[19] Suhas, P.J.M. Carrott, M.M.L. Ribeiro Carrott, Lignin - from natural adsorbent to activated carbon: a review, Bioresour. Technol. (2007), https://doi.org/10.1016/j.biortech.2006.08.008.
[20] F.L. Braghiroli, G. Amaral-Labat, A.F.N. Boss, C. Lacoste, A. Pizzi, Tannin gels and their carbon derivatives: a review, Biomolecules 9 (2019) 587, https://doi.org/10.3390/biom9100587.
[21] D.K. Sam, E.K. Sam, A. Durairaj, X. Lv, Z. Zhou, J. Liu, Synthesis of biomass-based carbon aerogels in energy and sustainability, Carbohydr. Res. 491 (2020) 107986, https://doi.org/10.1016/j.carres.2020.107986.
[22] B.S. Yang, K.-Y. Kang, M.-J. Jeong, Preparation of lignin-based carbon aerogels as biomaterials for nano-supercapacitor, J. Kor. Phys. Soc. 71 (2017) 478–482, https://doi.org/10.3938/jkps.71.478.
[23] H. Zhuo, Y. Hu, X. Tong, L. Zhong, X. Peng, R. Sun, Sustainable hierarchical porous carbon aerogel from cellulose for high-performance supercapacitor and CO2 capture, Ind. Crops Prod. 87 (2016) 229–235, https://doi.org/10.1016/j.indcrop.2016.04.041.
[24] H. Zhao, Y. Chen, Q. Peng, Q. Wang, G. Zhao, Catalytic activity of MOF(2Fe/Co)/carbon aerogel for improving H2O2 and [rad] OH generation in solar photo–electro–Fenton process, Appl. Catal. B Environ. 203 (2017) 127–137, https://doi.org/10.1016/j.apcatb.2016.09.074.
[25] B. Medronho, B. Lindman, Brief overview on cellulose dissolution/regeneration interactions and mechanisms, Adv. Colloid Interface Sci. 222 (2015) 502–508, https://doi.org/10.1016/j.cis.2014.05.004.
[26] R.B. Valim, R.M. Reis, P.S. Castro, A.S. Lima, R.S. Rocha, M. Bertotti, M.R.V. Lanza, Electrogeneration of hydrogen peroxide in gas diffusion electrodes modified with tert-butyl-anthraquinone on carbon black support, Carbon N. Y. 61 (2013) 236–244, https://doi.org/10.1016/j.carbon.2013.04.100.
[27] R.B. Valim, J.C. Lourenço, L.C. Trevelin, A.F. Siqueira, L.A. Rodrigues, R.S. Rocha, M.R.V. Lanza, Using GDE modified with mixed Ru[sbnd]Nb oxides for Ciprofloxacin degradation via the electro-Fenton process and its prediction model, J. Water Process Eng. 55 (2023) 104113, https://doi.org/10.1016/j.jwpe.2023.104113.
[28] N.P. de Moraes, F.H.C. Boldrin, T.M.B. Campos, G.P. Thim, Y. Lianqing, M.R. de Vasconcelos Lanza, L.A. Rodrigues, Black-wattle tannin/kraft lignin H3PO4-activated carbon xerogels as excellent and sustainable adsorbents, Int. J. Biol. Macromol. 227 (2023) 58–70, https://doi.org/10.1016/j.ijbiomac.2022.12.125.
[29] Y. Lin, Chen Huang, Caoxing Huang, Y. Deng, X. Zou, W. Ma, G. Fang, A.J. Ragauskas, Cellulose regulated lignin/cellulose-based carbon materials with hierarchical porous structure for energy storage, Adv. Compos. Hybrid Mater. 7 (2024) 1–13, https://doi.org/10.1007/s42114-024-00850-5.
[30] B. Li, J. Hu, H. Xiong, Y. Xiao, Application and properties of microporous carbons activated by ZnCl2: adsorption behavior and activation mechanism, ACS Omega 5 (2020) 9398–9407, https://doi.org/10.1021/acsomega.0c00461.
[31] J. Li, X. Bai, Y. Fang, Y. Chen, X. Wang, H. Chen, H. Yang, Comprehensive mechanism of initial stage for lignin pyrolysis, Combust. Flame 215 (2020) 1–9, https://doi.org/10.1016/j.combustflame.2020.01.016.
[32] D. Zhang, T. Liu, K. Yin, C. Liu, Y. Wei, Selective H2O2 production on N-doped porous carbon from direct carbonization of metal organic frameworks for electro-Fenton mineralization of antibiotics, Chem. Eng. J. 383 (2020), https://doi.org/10.1016/j.cej.2019.123184.
[33] Q. Zhang, M. Zhou, G. Ren, Yawei Li, Yanchun Li, X. Du, Highly efficient electrosynthesis of hydrogen peroxide on a superhydrophobic three-phase interface by natural air diffusion, Nat. Commun. 11 (2020) 1–11, https://doi.org/10.1038/s41467-020-15597-y.
[34] V. Librando, Z. Minniti, S. Lorusso, Ancient and modern paper characterization by FTIR and Micro-Raman spectroscopy, Conserv. Sci. Cult. Herit. 11 (2011) 249–268, https://doi.org/10.6092/issn.1973-9494/2700.
[35] X. Liao, C. Chen, R. Zhou, Q. Huang, Q. Liang, Z. Huang, Y. Zhang, H. Hu, Y. Liang, Comparison of N-doped carbon dots synthesized from the main components of plants including cellulose, lignin, and xylose: characterized, fluorescence mechanism, and potential applications, Dyes Pigments 183 (2020) 108725, https://doi.org/10.1016/j.dyepig.2020.108725.
[36] N.P. de Moraes, A. de Siervo, T.O. Silva, R. da Silva Rocha, D.A. Reddy, Y. Lianqing, M.R. de Vasconcelos Lanza, L.A. Rodrigues, Kraft lignin-based carbon xerogel/zinc oxide composite for 4-chlorophenol solar-light photocatalytic degradation: effect of pH, salinity, and simultaneous Cr(VI) reduction, Environ. Sci. Pollut. Res. 30 (2023) 8280–8296, https://doi.org/10.1007/s11356-022-22825-z.
[37] Y. Gokce, Z. Aktas, Nitric acid modification of activated carbon produced from waste tea and adsorption of methylene blue and phenol, Appl. Surf. Sci. 313 (2014) 352–359, https://doi.org/10.1016/j.apsusc.2014.05.214.
[38] N. Cabezudo, J. Sun, B. Andi, F. Ding, D. Wang, W. Chang, X. Luo, B.B. Xu, Enhancement of surface wettability via micro- and nanostructures by single point diamond turning, Nanotechnol. Precis. Eng. 2 (2019) 8–14, https://doi.org/10.1016/j.npe.2019.03.008.
[39] N. Li, C. Huang, X. Wang, Y. Feng, J. An, Electrosynthesis of hydrogen peroxide via two-electron oxygen reduction reaction: a critical review focus on hydrophilicity/hydrophobicity of carbonaceous electrode, Chem. Eng. J. 450 (2022) 138246, https://doi.org/10.1016/j.cej.2022.138246.
[40] D. Paluch, A. Bazan-Wozniak, R. Pietrzak, Methyl red adsorption on biochar obtained by physical activation of caraway seeds with carbon dioxide, ChemPhysChem (2024), https://doi.org/10.1002/cphc.202300821.
[41] N.P. de Moraes, F.A. Torezin, G.V. Jucá Dantas, J.G.M. de Sousa, R.B. Valim, R. da Silva Rocha, R. Landers, M.L.C.P. da Silva, L.A. Rodrigues, TiO2/Nb2O5/carbon xerogel ternary photocatalyst for efficient degradation of 4-chlorophenol under solar light irradiation, Ceram. Int. 46 (2020) 14505–14515, https://doi.org/10.1016/j.ceramint.2020.02.249.
[42] G. Liu, M. Feng, M. Tayyab, J. Gong, M. Zhang, M. Yang, K. Lin, Direct and efficient reduction of perfluorooctanoic acid using bimetallic catalyst supported on carbon, J. Hazard Mater. 412 (2021) 125224, https://doi.org/10.1016/j.jhazmat.2021.125224.
[43] E. Pamula, P.G. Rouxhet, Bulk and surface chemical functionalities of type III PAN-based carbon fibres, Carbon N. Y. (2003), https://doi.org/10.1016/S0008-6223(03)00177-5.
[44] A. Ghosh, S. Ghosh, G.M. Seshadhri, S. Ramaprabhu, Green synthesis of nitrogen-doped self-assembled porous carbon-metal oxide composite towards energy and environmental applications, Sci. Rep. 9 (2019) 1–13, https://doi.org/10.1038/s41598-019-41700-5.
[45] E.S.F. Cardoso, G.V. Fortunato, I. Palm, E. Kibena-Põldsepp, A.S. Greco, J.L.R. Júnior, A. Kikas, M. Merisalu, V. Kisand, V. Sammelselg, K. Tammeveski, G. Maia, Effects of N and O groups for oxygen reduction reaction on one- and two-dimensional carbonaceous materials, Electrochim. Acta 344 (2020), https://doi.org/10.1016/j.electacta.2020.136052.
[46] L. Li, C. Tang, Y. Zheng, B. Xia, X. Zhou, H. Xu, S.Z. Qiao, Tailoring selectivity of electrochemical hydrogen peroxide generation by tunable pyrrolic-nitrogen-carbon, Adv. Energy Mater. 10 (2020) 1–10, https://doi.org/10.1002/aenm.202000789.
[47] D. Iglesias, A. Giuliani, M. Melchionna, S. Marchesan, A. Criado, L. Nasi, M. Bevilacqua, C. Tavagnacco, F. Vizza, M. Prato, P. Fornasiero, N-doped graphitized carbon nanohorns as a forefront electrocatalyst in highly selective O2 reduction to H2O2, Chem 4 (2018) 106–123, https://doi.org/10.1016/j.chempr.2017.10.013.
[48] G. Li, Y. Zhang, Highly selective two-electron oxygen reduction to generate hydrogen peroxide using graphite felt modified with N-doped graphene in an electro-Fenton system, New J. Chem. 43 (2019) 12657–12667, https://doi.org/10.1039/C9NJ02601K.
[49] H. Wu, Z. Dong, J. Sun, K. Ding, Boosting the adsorption capacity of activated carbon prepared from Amygdalus communis shells using physicochemical co-activation method, Biomass Convers. Biorefinery 14 (2024) 18121–18131, https://doi.org/10.1007/s13399-023-04093-0.
[50] X. He, K.B. Male, P.N. Nesterenko, D. Brabazon, B. Paull, J.H.T. Luong, Adsorption and desorption of methylene blue on porous carbon monoliths and nanocrystalline cellulose, ACS Appl. Mater. Interfaces (2013), https://doi.org/10.1021/am403222u.
[51] R.B. Valim, L.C. Trevelin, D.C. Sperandio, J.F. Carneiro, M.C. Santos, L.A. Rodrigues, R.S. Rocha, M.R.V. Lanza, Using carbon black modified with Nb2O5 and RuO2 for enhancing selectivity toward H2O2 electrogeneration, J. Environ. Chem. Eng. 9 (2021) 106787, https://doi.org/10.1016/j.jece.2021.106787.
[52] T. Oliveira Silva, G. de Oliveira Santiago Santos, R. Colombo, M.R. de Vasconcelos Lanza, M.A. Rodrigo Rodrigo, Degradation of diethyl phthalate by

photolysis of hydrogen peroxide electrogenerated using a Printex L6 carbon modified with Benzophenone cathode in an improved tangential flow cell, Process Saf. Environ. Prot. 188 (2024) 86–95, https://doi.org/10.1016/j.psep.2024.05.092.